Mathematics in Applied Sciences and Engineering
Volume **3**, Number **1**, March **2022**, pp.**60-85**
https://ojs.lib.uwo.ca/mase
https://doi.org/10.5206/mase/14537

HOW DOES THE LATENCY PERIOD IMPACT THE MODELING OF COVID-19 TRANSMISSION DYNAMICS?

BEN PATTERSON AND JIN WANG

Abstract. We introduce two mathematical models based on systems of differential equations to investigate the relationship between the latency period and the transmission dynamics of COVID-19. We analyze the equilibrium and stability properties of these models, and perform an asymptotic study in terms of small and large latency periods. We fit the models to the COVID-19 data in the U.S. state of Tennessee. Our numerical results demonstrate the impact of the latency period on the dynamical behaviors of the solutions, on the value of the basic reproduction numbers, and on the accuracy of the model predictions.

1. Introduction

The coronavirus disease 2019 (COVID-19), caused by severe acute respiratory syndrome coronavirus 2 (SARS-CoV-2), has been a global pandemic for almost two years. Despite tremendous efforts in disease control and management, particularly the development and deployment of efficacious vaccines, most countries and territories continue to struggle with the pandemic. As of December 2021, more than 270 million cases were reported throughout the world [43]. In the U.S. alone, COVID-19 already led to nearly 50 million cases and over 800 thousand deaths [38].

Mathematical and computational models, which have long been used in epidemiological research [4, 6, 13, 30], can help us better understand the transmission dynamics of COVID-19 so as to design more effective intervention strategies. A number of mathematical models for COVID-19 have been published (see, e.g., [16,17,19,20,27,29,33,34,36,37]). Most of these models are based on the susceptible-infectious-recovered (SIR) or susceptible-exposed-infectious-recovered (SEIR) compartmental framework. SIR and SEIR (and their variants), as two basic types of epidemic models, have been studied extensively and applied to numerous infectious diseases [13, 23].

A distinctive feature of COVID-19 not reflected by SIR and SEIR models, however, is that asymptomatic and pre-symptomatic infection is common; i.e., infected individuals could be contagious without showing any symptoms [10, 26, 28]. Individuals during this time interval, referred to as an incubation period, may not be aware of their infection at all (since they do not exhibit symptoms) and may easily transmit the disease to other people through movement and contact. This has been one of the important factors that lead to the fast spread of COVID-19. It is widely believed that the incubation period for COVID-19 could be as long as 14 days [38]. Quite a few publications have also estimated the mean incubation period for COVID-19. For example, a study for COVID-19 patients in China found that the median incubation period was 4.4 days before January 25, 2020 and 11.5 days after January 31, 2020 [21]. A meta-analysis in [9] showed that the mean incubation period of COVID-19 was 6.0 days globally from

2010 *Mathematics Subject Classification.* Primary 92D30, 92D25; Secondary 37N25, 34A34.
Key words and phrases. COVID-19, mathematical modeling, latency period, data fitting.
This work was partially supported by the National Institutes of Health under grant number 1R15GM131315.

December 2019 to May 2021. Another pooled estimate of the COVID-19 incubation period yielded 5.74 days [25].

A concept closely related to the incubation period is the latency period. While the incubation period measures the time between infection and onset of symptoms, the latency period represents the time from infection to infectiousness. The presence of asymptomatic infection for COVID-19 indicates that the incubation of the disease typically lasts longer than the latency [12, 24]. This is supported by clinical observations of COVID-19 patients that their mean incubation period was longer than their mean latency period [35]. A meta-analysis of reported data from seven countries found that the mean latency period was about 2.52 days [22]. Another study found that on average the peak infectivity of COVID-19 occurred about 1 day before symptom onset [21]. The specific length of the latency period, however, varies from individual to individual, which contributes to a highly heterogeneous pattern in the course of COVID-19 infection.

The main goal of this paper is to investigate the impact of the latency period on the transmission dynamics modeling of COVID-19. Among the large number of mathematical and computational models published thus far for COVID-19, very few have been devoted to this point. Sadun [27] considered the effects of latency on the basic reproduction number of COVID-19 and estimated the fraction of the population that would become infected in the long run. Liu et al. [20] incorporated the latency period into two differential equation-based models, including one with a time delay, and fitted the models to COVID-19 data in China. Despite these studies, our understanding of the relationship between the latency period and disease transmission and spread remains inadequate, and our current knowledge is limited regarding the interplay between the asymptomatic infection and the latency in shaping the transmission dynamics of COVID-19.

To address this issue, we will introduce two simple models in this work, denoted as SAIR and SEAIR, respectively. The first model consists of the susceptible (S), asymptomatic infectious (A), symptomatic infectious (I), and recovered (R) individuals. The second model includes an additional compartment E for the exposed, or latent, individuals. We will then compare the dynamics of these two models, with a focus on the different dynamical behaviors introduced by the presence of the E compartment. In particular, we will use perturbation theory [3, 14, 15] to analyze the relationship between the two models. Additionally, we will apply both models to the COVID-19 cases in the U.S. state of Tennessee, using data from the Tennessee Department of Health [41]. Through data fitting and numerical simulation, we will demonstrate the connection between the SAIR and SEAIR models and their different dynamical behaviors in a real-world application.

The remainder of this article is organized as follows. In Section 2, the SAIR and SEAIR models are formulated, and the main results of their equilibrium analysis are summarized (with details provided in the Appendices). In Section 3, an asymptotic analysis is conducted for the SEAIR model in terms of small and large latency periods. In Section 4, data fitting and numerical simulation results for both models are presented. Finally, some discussion is made in Section 5 to conclude the paper.

2. Model formulation and equilibrium dynamics

2.1. **SAIR model.** To study the transmission behavior of COVID-19, we consider the following SAIR system of differential equations:

$$\begin{aligned}
\frac{dS}{dt} &= \Lambda - \beta_A SA - \beta_I SI - \mu S,\\
\frac{dA}{dt} &= \beta_A SA + \beta_I SI - (\alpha + \gamma_1 + \mu)A,\\
\frac{dI}{dt} &= \alpha A - (w + \gamma_2 + \mu)I,\\
\frac{dR}{dt} &= \gamma_1 A + \gamma_2 I - \mu R,
\end{aligned} \tag{2.1}$$

where S, A, I, and R are the compartments for susceptible, asymptomatic infectious, symptomatic infectious, and recovered individuals, respectively. Susceptible individuals become infected by contacting infectious individuals. Infected individuals first become asymptomatic infectious; some of them will develop symptoms later, while others will remain asymptomatic over the entire course of their infection. The parameter Λ is the population influx rate, β_A and β_I are the rates of transmission from asymptomatic and symptomatic infections, respectively, μ is the natural death rate, α^{-1} is the incubation period (so α is the rate of transfer from A to I), γ_1 is the rate at which individuals recover from asymptomatic infection, γ_2 is the rate at which individuals recover from symptomatic infection, and w is the disease-induced death rate. It is assumed that all of these parameters are positive constants.

Using the standard next-generation matrix analysis (with details provided in Appendix A), we obtain the basic reproduction number for the SAIR model (2.1) as

$$\mathcal{R}_0^{\mathrm{SAIR}} = \frac{\beta_A \Lambda}{\mu(\alpha + \gamma_1 + \mu)} + \frac{\alpha\beta_I \Lambda}{\mu(\alpha + \gamma_1 + \mu)(w + \gamma_2 + \mu)} := \mathcal{R}_1^{\mathrm{SAIR}} + \mathcal{R}_2^{\mathrm{SAIR}}, \tag{2.2}$$

where $\mathcal{R}_1^{\mathrm{SAIR}}$ and $\mathcal{R}_2^{\mathrm{SAIR}}$ quantify the contributions from asymptomatic and symptomatic infections, respectively, to the disease transmission risk.

Meanwhile, from an equilibrium analysis (Appendix B), we can establish the following results for the SAIR model: when $\mathcal{R}_0^{\mathrm{SAIR}} < 1$, there is a unique disease-free equilibrium (DFE): $(\Lambda/\mu, 0, 0, 0)$, which is locally asymptotically stable; when $\mathcal{R}_0^{\mathrm{SAIR}} > 1$, the DFE is unstable, and there is a unique endemic equilibrium which is locally asymptotically stable.

2.2. **SEAIR model.** Next, we consider the following SEAIR system for the transmission dynamics of COVID-19:

$$\begin{aligned}
\frac{dS}{dt} &= \Lambda - \beta_A SA - \beta_I SI - \mu S,\\
\frac{dE}{dt} &= \beta_A SA + \beta_I SI - (v + \mu)E,\\
\frac{dA}{dt} &= vE - (\alpha + \gamma_1 + \mu)A,\\
\frac{dI}{dt} &= \alpha A - (w + \gamma_2 + \mu)I\\
\frac{dR}{dt} &= \gamma_1 A + \gamma_2 I - \mu R,
\end{aligned} \tag{2.3}$$

where the additional compartment E represents exposed individuals who are infected but not yet infectious. This model differs from our previous SAIR model in that infected individuals will not begin infecting other people immediately, instead experiencing a latency period where they neither show symptoms nor infect others. The parameter v denotes the rate of transfer from E to A; i.e., v^{-1} represents the latency period. Other parameters have the same meanings as those in the SAIR model.

Using the next-generation matrix analysis again (Appendix A), we obtain the basic reproduction number for the SEAIR model (2.3) as

$$\mathcal{R}_0^{\text{SEAIR}} = \frac{v\beta_A\Lambda}{\mu(v+\mu)(\alpha+\gamma_1+\mu)} + \frac{v\alpha\beta_I\Lambda}{\mu(v+\mu)(\alpha+\gamma_1+\mu)(w+\gamma_2+\mu)} := \mathcal{R}_1^{\text{SEAIR}} + \mathcal{R}_2^{\text{SEAIR}}, \tag{2.4}$$

where $\mathcal{R}_1^{\text{SEAIR}}$ and $\mathcal{R}_2^{\text{SEAIR}}$ measure the contributions from asymptomatic and symptomatic infections, respectively, to the disease risk in the current SEAIR model.

Similarly, an equilibrium analysis (Appendix C) yields the following results for the SEAIR model: when $\mathcal{R}_0^{\text{SEAIR}} < 1$, there is a unique disease-free equilibrium $(\Lambda/\mu,\, 0,\, 0,\, 0,\, 0)$, which is locally asymptotically stable; when $\mathcal{R}_0^{\text{SEAIR}} > 1$, the DFE is unstable, and there is a unique endemic equilibrium which is locally asymptotically stable.

3. Asymptotic analysis

From equations (2.2) and (2.4), it is straightforward to observe that when $v \to 0$, $\mathcal{R}_0^{\text{SEAIR}} \to 0$; when $v \to \infty$, $\mathcal{R}_0^{\text{SEAIR}} \to \mathcal{R}_0^{\text{SAIR}}$. These suggest special dynamical behaviors with respect to small and large values of v. To explore such dynamical properties, we conduct an asymptotic analysis for the SEAIR model in what follows.

When $v = 0$, the SEAIR system (2.3) becomes

$$\begin{aligned}
\frac{dS}{dt} &= \Lambda - \beta_A SA - \beta_I SI - \mu S,\\
\frac{dE}{dt} &= \beta_A SA + \beta_I SI - \mu E,\\
\frac{dA}{dt} &= -(\alpha+\gamma_1+\mu)A,\\
\frac{dI}{dt} &= \alpha A - (w+\gamma_2+\mu)I.
\end{aligned} \tag{3.1}$$

We have dropped the equation for R, since it is not needed in the analysis. Given an initial condition $(S, E, A, I) = \big(S(0),\, E(0),\, A(0),\, I(0)\big)$ at $t = 0$, it can be easily verified that the solution of system (3.1) satisfies

$$A(t) = A(0)e^{-(\alpha+\gamma_1+\mu)t}, \quad I(t) = \frac{\alpha A(0)e^{-(\alpha+\gamma_1+\mu)t}}{w+\gamma_2-\alpha-\gamma_1} + \Big[I(0) - \frac{\alpha A(0)}{w+\gamma_2-\alpha-\gamma_1}\Big]e^{-(w+\gamma_2+\mu)t}$$

and

$$S(t) + E(t) = \frac{\Lambda}{\mu} + \big[S(0) + E(0) - \frac{\Lambda}{\mu}\big]e^{-\mu t}.$$

When $t \to \infty$, $A(t) \to 0$ and $I(t) \to 0$, which implies that $E(t) \to 0$ based on the second equation of system (3.1). Hence, when $t \to \infty$, any solution of system (3.1) approaches the disease-free equilibrium $\big(\frac{\Lambda}{\mu},\, 0,\, 0,\, 0\big)$.

By the continuous dependence on parameters for the solutions of the differential equations, we obtain that when $v \to 0$, all solutions of the original SEAIR system will approach the DFE. In other words, the case with a very large latency period (i.e., $v \to 0$) can be treated as a regular perturbation [3] to the differential system. The result can be easily expected from a biological perspective: when the latency period is sufficiently long, the infection will not spread out and will be eradicated. This is consistent with our observation that $\mathcal{R}_0^{\text{SEAIR}} \to 0$ as $v \to 0$.

The case with a very small latency period (i.e., $v \to \infty$), however, represents a singular perturbation. To analyze this scenario, we let

$$\varepsilon = \frac{1}{v}$$

be the length of the latency period, and examine the solution of the SEAIR system for a small $\varepsilon > 0$ using techniques of singular perturbations [5, 14, 15].

We first re-write system (2.3) as

$$\begin{aligned} \frac{dS}{dt} &= \Lambda - \beta_A SA - \beta_I SI - \mu S, \\ \frac{dI}{dt} &= \alpha A - (w + \gamma_2 + \mu) I, \\ \frac{d}{dt}(E + A) &= \beta_A SA + \beta_I SI - \mu E - (\alpha + \gamma_1 + \mu) A, \\ \varepsilon \frac{dE}{dt} &= \varepsilon \big[\beta_A SA + \beta_I SI - \mu E\big] - E, \end{aligned} \tag{3.2}$$

where we have replaced the equation for A with an equation for $E+A$, obtained by adding the second and third equations in the original system, and where we have multiplied ε on both sides of the E equation. The first three equations in system (3.2) are on a 'slow' time scale, compared to the last equation which is on a 'fast' scale due to the multiplication of a small ε to the time derivative.

To proceed, we introduce a fast time variable τ by

$$\tau = \frac{t}{\varepsilon}.$$

Then system (3.2) can be transformed to

$$\begin{aligned} \frac{dS}{d\tau} &= \varepsilon\big(\Lambda - \beta_A SA - \beta_I SI - \mu S\big), \\ \frac{dI}{d\tau} &= \varepsilon\big[\alpha A - (w + \gamma_2 + \mu) I\big], \\ \frac{d}{d\tau}(E + A) &= \varepsilon\big[\beta_A SA + \beta_I SI - \mu E - (\alpha + \gamma_1 + \mu) A\big], \\ \frac{dE}{d\tau} &= \varepsilon\big[\beta_A SA + \beta_I SI - \mu E\big] - E. \end{aligned} \tag{3.3}$$

Since system (3.2) is formulated by the slow time variable t, we refer to it as the slow system. In contrast, system (3.3) is in terms of the fast time variable τ, and we refer to it as the fast system. These two systems have the same phase portraits for $\varepsilon > 0$, but they have different limit behaviors at $\varepsilon = 0$: the limit of the slow system describes the dynamics on a large time interval away from 0, whereas the limit of the fast system describes the dynamics for a small neighborhood of time 0. Details are provided below.

Setting $\varepsilon = 0$ in system (3.2), we obtain the reduced slow system (or, the slow limit system)

$$\begin{aligned} \frac{dS}{dt} &= \Lambda - \beta_A SA - \beta_I SI - \mu S, \\ \frac{dI}{dt} &= \alpha A - (w + \gamma_2 + \mu) I, \\ \frac{d}{dt}(E + A) &= \beta_A SA + \beta_I SI - \mu E - (\alpha + \gamma_1 + \mu) A, \\ E &= 0. \end{aligned} \tag{3.4}$$

Substitution of the last equation ($E = 0$) into the third equation of system (3.4) yields

$$\begin{aligned}\frac{dS}{dt} &= \Lambda - \beta_A SA - \beta_I SI - \mu S,\\ \frac{dI}{dt} &= \alpha A - (w + \gamma_2 + \mu)I,\\ \frac{dA}{dt} &= \beta_A SA + \beta_I SI - (\alpha + \gamma_1 + \mu)A.\end{aligned} \tag{3.5}$$

System (3.5) is identical to the SAIR model (2.1), where the equation for R does not need to be included. Hence, when $\varepsilon \to 0$, the dynamical behavior of the SEAIR model will approach that of the SAIR model as long as the time t is not very close to 0. This scenario is relevant to our research interest, since the focuses in most epidemiological applications are how an epidemic would spread after its onset and what would be its long-term progression, and those are concerned with relatively large time.

This result is consistent with our previous observation that $\mathcal{R}_0^{\text{SEAIR}} \to \mathcal{R}_0^{\text{SAIR}}$ when $v \to \infty$. The biological interpretation is that when the latency period is sufficiently short, the impact of the latency could be disregarded. Consequently, the dynamics of the disease transmission could be described by the SAIR model, without incorporating the E compartment.

On the other hand, when $\varepsilon \to 0$, the dynamical behavior of the SEAIR model very close to the time at 0 would be described by the limit of the fast system (3.3). Setting $\varepsilon = 0$ in (3.3) leads to the reduced fast system (or, the fast limit system)

$$\begin{aligned}\frac{dS}{d\tau} &= 0,\\ \frac{dI}{d\tau} &= 0,\\ \frac{d}{d\tau}(E + A) &= 0,\\ \frac{dE}{d\tau} &= -E.\end{aligned} \tag{3.6}$$

System (3.6) yields

$$S(\tau) = S(0), \quad I(\tau) = I(0), \quad A(\tau) = A(0) + E(0) - E(0)e^{-\tau}, \quad E(\tau) = E(0)e^{-\tau}.$$

In particular, $E(\tau)$ will quickly decrease to 0 when τ is increasing. Hence, in a small neighborhood of time 0, the solution for $E(\tau)$ exhibits a rapid change. This is an analogue to a boundary layer solution in fluid dynamics [2, 32].

We will use numerical simulation in the next section to verify some of these asymptotic predictions. In particular, we will quantify the impact of the latency period on the dynamics of the SEAIR model using real data.

4. Numerical simulation

4.1. **Fitting of data.** We apply our models to the COVID-19 data in the U.S. state of Tennessee in the period between January 1st, 2021 and June 30th, 2021. The most recent estimate from the U.S. Census Bureau puts the total population of Tennessee at N = 6,829,174 [42]. Since the time period we consider is short, we assume that immigration and emigration are equal and that the natural birth rate is the same as the natural death rate μ. The natural death rate is defined as the reciprocal of the average life expectancy in the state, which is 75.5 years [1]. We then define the population influx rate as the product of the natural birth rate and total population, $\Lambda = \mu N$. Meanwhile, we calculate the recovery rate of asymptomatic infection (γ_1), the recovery rate of symptomatic infection (γ_2), and the incubation rate (α) by the reciprocal of the asymptomatic infection period, the symptomatic infection period, and

the incubation period, respectively, reported in [8]. Similarly, we calculate the latency rate (v) using the reciprocal of the average latency period reported in [22]. All these parameter values used in this section are provided in Table 1.

The remaining parameters are the transmission rates β_A and β_I, and the disease-induced death rate w. These three parameters may vary significantly from place to place. Particularly, a sensitivity analysis (Appendix D) indicates that β_A and β_I are among the most sensitive parameters for the basic reproduction numbers of both models. Hence, we will estimate the values of these three parameters by fitting our models to the infection data reported from Tennessee Department of Health [40].

TABLE 1. Values of parameters

Parameter	Definition	Value	Source
Λ	Influx Rate	247.815 persons per day	[1, 42]
μ	Natural death rate	3.629×10^{-5} per day	[1]
α^{-1}	Incubation period	4 days	[8]
γ_1^{-1}	Asymptomatic recovery period	9.5 days	[8]
γ_2^{-1}	Symptomatic recovery period	18.07 days	[8]
v^{-1}	Latency period	2.52 days	[22]
β_A	Asymptomatic transmission rate	found by data fitting	-
β_I	Symptomatic transmission rate	found by data fitting	-
w	Disease-induced death rate	found by data fitting	-

We first conduct data fitting for the SAIR model (2.1) based on the reported data from January 1st, 2021 to June 30th, 2021. We fit the number of cumulative confirmed cases using the standard least squares method. We assume that cases are not detected prior to symptom onset, and that fully asymptomatic cases are not taken into account in the recorded number of active cases. The numbers for the active cases and the susceptible and recovered people on January 1st, 2021 are available [40] and they are used in our initial condition. To obtain the initial condition for the number of asymptomatic cases, we use the estimate given by CDC that asymptomatic cases make up about 30% of all active cases [39]; that is, $A(0) = \frac{3}{7} \times I(0)$. Thus, our initial condition is given by $(S(0), A(0), I(0), R(0)) = (6218190, 25642, 59831, 525511)$. From the numerical solution, the number of cumulative confirmed cases at time t is approximated by

$$I(t) + R(t) + \int_0^t wI(\tau)\, d\tau\,,$$

where the first term represents the number of active infections, the second term represents the number of infected individuals that have recovered, and the third term represents the number of disease-induced deaths, as of time t. Table 2 contains the results from fitting the cumulative cases by the SAIR model for β_A, β_I and w, as well as their 95% confidence intervals. The normalized mean square error for this fitting is found to be 0.00023.

TABLE 2. Parameter estimates for the SAIR model

Parameter	Resultant Value	95% Confidence Interval
β_A	3.01×10^{-8}/person/day	$(2.78 \times 10^{-8}, 3.23 \times 10^{-8})$
β_I	4.59×10^{-9}/person/day	$(4.53 \times 10^{-9}, 4.66 \times 10^{-9})$
w	0.012/day	(0.000, 0.034)

Using these parameters, we calculate the basic reproduction number of the SAIR model and obtain $\mathcal{R}_0^{\text{SAIR}} = 0.907$, where $\mathcal{R}_0^{\text{SAIR}}$ is defined in equation (2.2). Broken down into two parts, we have $\mathcal{R}_1^{\text{SAIR}} =$

0.578, and $\mathcal{R}_2^{\mathrm{SAIR}} = 0.329$. Each of the two values quantifies a different route of disease transmission, with $\mathcal{R}_1^{\mathrm{SAIR}}$ representing the risk of transmission from asymptomatic individuals and $\mathcal{R}_2^{\mathrm{SAIR}}$ representing the risk of transmission from symptomatic individuals. From these values, we immediately observe the following: (1) The basic reproduction number $\mathcal{R}_0^{\mathrm{SAIR}}$ is lower than unity, indicating that the epidemic was decaying during the time period of our consideration. This is evidenced by the fact that the reported number of active cases in Tennessee decreased from almost 60,000 on January 1st, 2021 to about 1,200 on June 30th, 2021 [40]. The significant reduction of cases was most likely resulting from the vaccination campaign which started in the U.S. from mid-December 2020. (2) Between the two components of the basic reproduction number, $\mathcal{R}_1^{\mathrm{SAIR}} > \mathcal{R}_2^{\mathrm{SAIR}}$, indicating a higher disease risk from the group of asymptomatic infectious individuals. This is due to the fact that fewer intervention steps are taken to reduce the chance of virus spread, including quarantine or hospitalization, when an individual is not currently experiencing symptoms.

Figure 1 visualizes the fitting results for the number of cumulative cases based on the SAIR model and the parameter values provided in Tables 1 and 2. Figure 2 shows the simulation results for the asymptomatic and symptomatic infectious individuals in Tennessee during this time period that starts from January 1st, 2021.

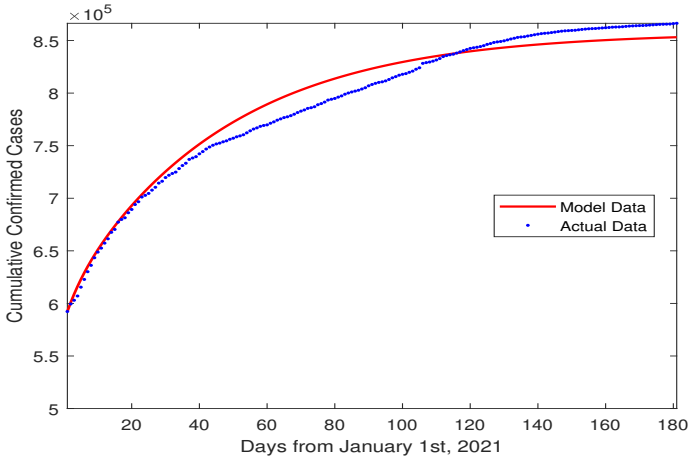

FIGURE 1. A comparison of the cumulative confirmed cases in Tennessee from January 1st, 2021 to June 30th, 2021 and the results of the SAIR model simulation using the known and fitted parameter values from Tables 1 and 2.

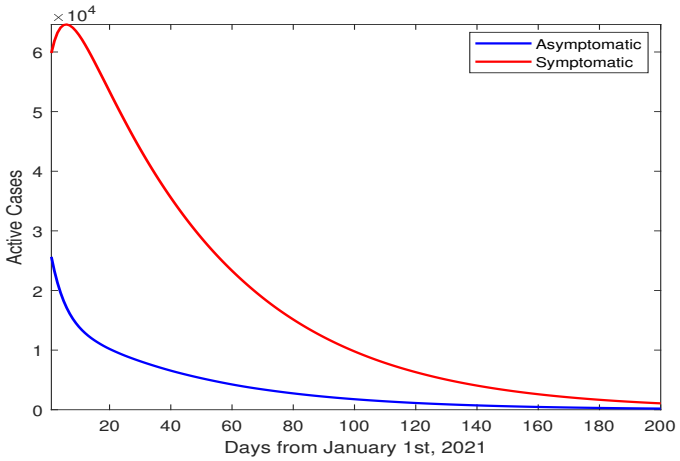

FIGURE 2. SAIR model simulation results showing the number of individuals in the asymptomatic and symptomatic infectious compartments for the time period starting from January 1st, 2021, based on the parameter values from Tables 1 and 2.

Next, we conduct data fitting to the SEAIR mode (2.3) and estimate the values of β_A, β_I, and w using the Tennessee COVID-19 data for the same 6-month period (from January 1st, 2021 to June 30th, 2021). The initial condition is given by $(S(0), E(0), A(0), I(0), R(0)) = (6198190,\ 20000,\ 25642,\ 59831,\ 525511)$, where we estimate that the number of exposed individuals to be 20,000 initially. Table 3 displays the results from fitting for β_A, β_I, and w, as well as their 95% confidence intervals. The normalized mean square error in this case is found to be 0.00089.

TABLE 3. Parameter estimates for the SEAIR model

Parameter	Resultant Value	95% Confidence Interval
β_A	2.98×10^{-8}/person/day	$(2.91 \times 10^{-8},\ 3.05 \times 10^{-8})$
β_I	4.56×10^{-9}/person/day	$(4.43 \times 10^{-9},\ 4.70 \times 10^{-9})$
w	0.013/day	(0.009, 0.016)

Using these parameters, we calculate the basic reproduction number of the SEAIR model and obtain $\mathcal{R}_0^{\text{SEAIR}} = 0.894$, with $\mathcal{R}_1^{\text{SEAIR}} = 0.573$ and $\mathcal{R}_1^{\text{SEAIR}} = 0.321$. We observe a similar patten as that of the SAIR model; i.e., $\mathcal{R}_0^{\text{SEAIR}} < 1$ and $\mathcal{R}_1^{\text{SEAIR}} > \mathcal{R}_2^{\text{SEAIR}}$. Meanwhile, Figure 3 illustrates the fitting results for the number of cumulative cases based on the SEAIR model, and Figure 4 displays the simulation results for the exposed (or, latent), asymptomatic, and symptomatic individuals during this time period starting from January 1st, 2021. We see that the curves for the asymptomatic and symptomatic individuals in Figure 4 show a similar behavior as that in Figure 2. We will make a careful comparison between the two models in the next section.

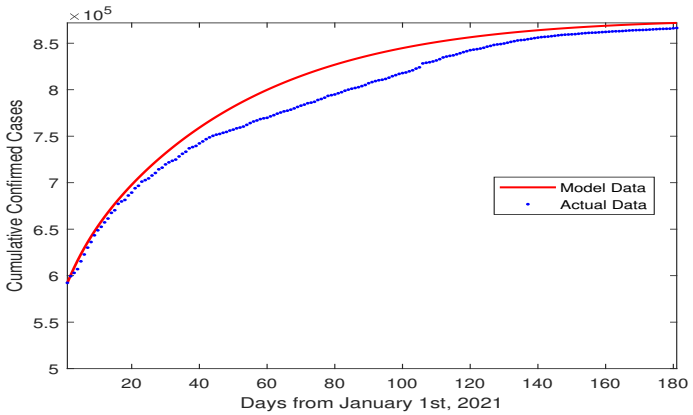

FIGURE 3. A comparison of the cumulative confirmed cases in Tennessee from January 1st, 2021 to June 30th, 2021 and the results of the SEAIR model simulation using the known and fitted parameter values from Tables 1 and 3.

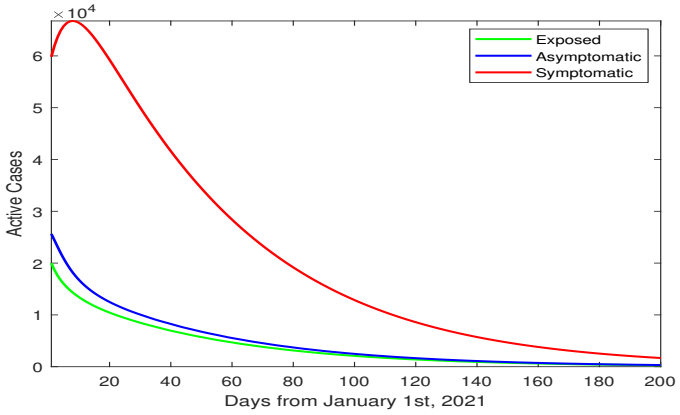

FIGURE 4. SEAIR model simulation results showing the number of individuals in the exposed, asymptomatic, and symptomatic compartments for the time period starting from January 1st, 2021, based on parameter values from Tables 1 and 3.

4.2. **Comparison of models.** Now we focus our attention on the comparison of the simulation results generated by the SAIR and SEAIR models. In particular, we examine how the value of the latency period impacts the numerical solution of the SEAIR model in reference to that of the SAIR model. To that end, we pick several different values of the latency period, with $v^{-1} = 0.1$ days, 1 day, 3 days, and 5 days, for the SEAIR model. We then run the SAIR model and the SEAIR model (for each given value of v) for the same time period from January 1st, 2021 to June 30th, 2021. Except for the parameter v, all the other parameters are fixed and their values are provided in Tables 1 and 3.

Figure 5 shows a comparison of the simulation results for the active asymptomatic cases generated by the SAIR model and the SEAIR models with different latency periods. Meanwhile, Figure 6 compares the the simulation results for the active symptomatic cases. We observe a clear pattern from these two figures: the shorter the latency period is, the closer the corresponding SEAIR curve is to the SAIR curve. This indicates that as the latency period approaches 0, the SEAIR model acts more similarly to the SAIR

model. An additional evidence is provided in Figure 7 where we plot the relative error of the SEAIR model with each given latency period for the total active cases, compared to those generated by the SAIR model. We clearly see that the relative error decreases when the latency period is reduced. When the latency period is 0.1 days, the relative error is already very close to 0. These findings provide a numerical demonstration of the asymptotic results derived in Section 3.

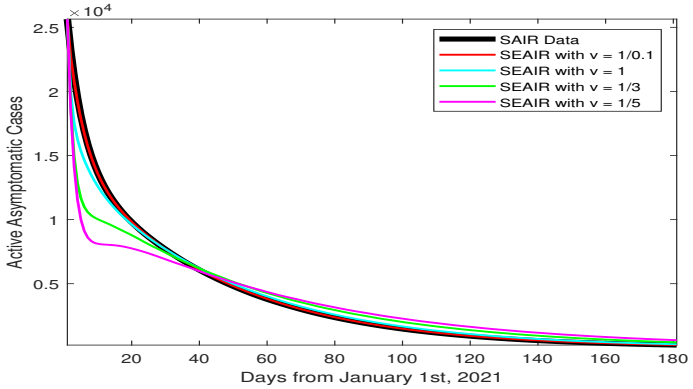

FIGURE 5. Simulation results for the active asymptomatic cases generated by the SAIR model and the SEAIR models with latency periods of 0.1 days, 1 day, 3 days, and 5 days.

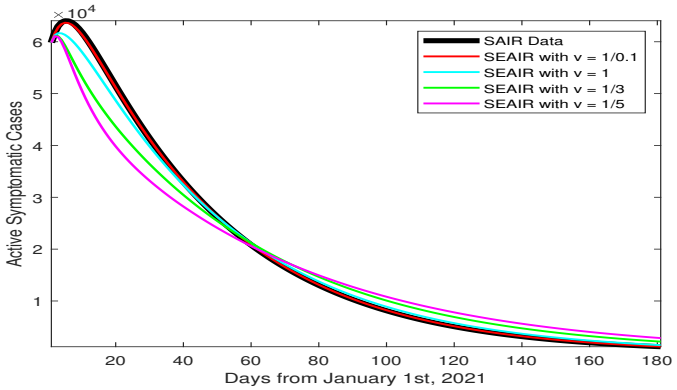

FIGURE 6. Simulation results for the active symptomatic cases generated by the SAIR model and the SEAIR models with latency periods of 0.1 days, 1 day, 3 days, and 5 days.

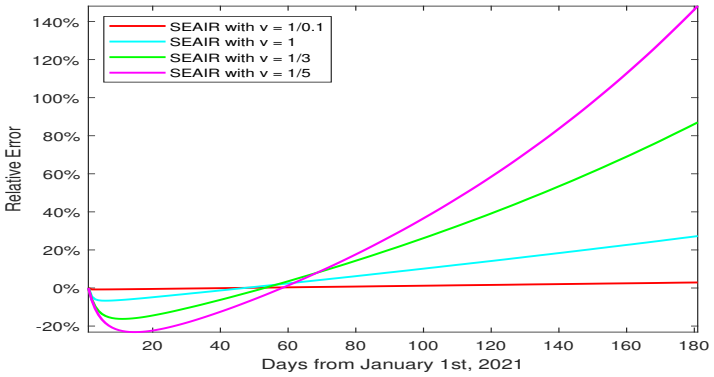

FIGURE 7. Relative error of total active cases generated by the SEAIR models with latency periods of 0.1 days, 1 day, 3 days, and 5 days, compared to those generated by the SAIR model.

In addition, we calculate the basic reproduction number for each model using these parameters and present the results in Table 4. The results numerically confirm that when the latency period approaches 0 (i.e., $\upsilon \to \infty$), $\mathcal{R}_0^{\text{SEAIR}} \to \mathcal{R}_0^{\text{SAIR}}$, as can be seen from the analytical expressions in equations (2.2) and (2.4). Another observation is that in all these cases, the values of the basic reproduction numbers are very close to each other. In fact, with a latency period of 5 days, $\mathcal{R}_0^{\text{SEAIR}}$ and $\mathcal{R}_0^{\text{SAIR}}$ only differ in the order of 10^{-4}, and with a latency period of 0.1 days, $\mathcal{R}_0^{\text{SEAIR}}$ and $\mathcal{R}_0^{\text{SAIR}}$ match each other up to 5 decimal digits. This is due to the fact that the basic reproduction number has a low sensitivity on the parameter υ (see the sensitivity analysis results in Appendix D). An implication is that, for the evaluation of the basic reproduction number for COVID-19, using the SAIR model or SEAIR model will not make a significant difference.

TABLE 4. Basic reproduction numbers for the SAIR model and the SEAIR model with latency periods of 0.1 days, 1 day, 3 days, and 5 days

Model	Basic reproduction number
SAIR	0.89158
SEAIR with $\upsilon = 1/0.1$ per day	0.89158
SEAIR with $\upsilon = 1/1$ per day	0.89155
SEAIR with $\upsilon = 1/3$ per day	0.89148
SEAIR with $\upsilon = 1/5$ per day	0.89142

4.3. **Accuracy of predictions.** Having compared the dynamical properties of the SAIR and SEAIR models, we now perform a more detailed study on the model output in terms of different latency periods, and assess the accuracy of these models and their abilities to predict future trends of COVID-19. For this purpose, we divide the 6-month time frame of our concern into two periods: (1) from January 1st, 2021 to May 31st, 2021, as the fitting period; and (2) from June 1st, 2021 to June 30th, 2021, as the testing period. We run each model with a different latency period to estimate the parameters β_A, β_I, and w using the reported infection data in the 5-month fitting period. Based on the fitted parameter values, a prediction is then generated from the model and compared to the reported data in the 1-month testing period.

Table 5 displays the parameter estimates in the fitting period using several values for the latency period: 0.1 days, 1 day, 2 days, 2.52 days, 3 days, and 4 days. We note that an average latency period

TABLE 5. Parameter estimates for different values of the latency period

Latency Period	Parameter	Resultant Value	95% Confidence Interval
0.1 days	β_A	2.85×10^{-8}/person/day	$(2.60 \times 10^{-8}, 3.11 \times 10^{-8})$
	β_I	4.60×10^{-9}/person/day	$(4.31 \times 10^{-9}, 4.89 \times 10^{-9})$
	w	0.013/day	$(0.004, 0.026)$
1 day	β_A	2.89×10^{-8}/person/day	$(2.71 \times 10^{-8}, 3.06 \times 10^{-8})$
	β_I	4.60×10^{-9}/person/day	$(4.35 \times 10^{-9}, 4.84 \times 10^{-9})$
	w	0.013/day	$(0.006, 0.020)$
2 days	β_A	2.93×10^{-8}/person/day	$(2.81 \times 10^{-8}, 3.06 \times 10^{-8})$
	β_I	4.60×10^{-9}/person/day	$(4.40 \times 10^{-9}, 4.80 \times 10^{-9})$
	w	0.013/day	$(0.009, 0.018)$
2.52 days	β_A	2.94×10^{-8}/person/day	$(2.83 \times 10^{-8}, 3.06 \times 10^{-8})$
	β_I	4.62×10^{-9}/person/day	$(4.45 \times 10^{-9}, 4.64 \times 10^{-9})$
	w	0.013/day	$(0.010, 0.017)$
3 days	β_A	2.95×10^{-8}/person/day	$(2.85 \times 10^{-8}, 3.05 \times 10^{-8})$
	β_I	4.66×10^{-9}/person/day	$(4.50 \times 10^{-9}, 4.81 \times 10^{-9})$
	w	0.013/day	$(0.011, 0.016)$
4 days	β_A	2.96×10^{-8}/person/day	$(2.87 \times 10^{-8}, 3.04 \times 10^{-8})$
	β_I	4.70×10^{-9}/person/day	$(4.56 \times 10^{-9}, 4.83 \times 10^{-9})$
	w	0.013/day	$(0.011, 0.015)$

of 2.52 days for COVID-19 was reported in [22]. Among these different latency periods, we pick $v^{-1} =$ 1 day, 2 days, 2.52 days, and 4 days, and present the numerical results for these four latency periods in Figure 8. On the left panel of Figure 8, we show the comparison between the actual data and the simulation results for the cumulative cases on both the fitting and testing periods, with each choice of the latency period. On the right panel of Figure 8, we plot the relative errors of the simulation results on the testing period, in reference to the actual data.

From Figure 8 (c) and (e), we observe that when the latency period is 2 days or 2.52 days, the simulation results are very close to the actual data in the testing period. This is confirmed by the plot of the relative errors on the right panel, (d) and (f), each of which shows an error close to 0. Furthermore, a careful examination of the right panel indicates that when the latency period is less than or equal to 2 days, the relative error remains negative (a pattern of undershooting in the testing period), and the magnitude of the error decreases when the latency period increases. On the other hand, when the latency period is larger than or equal to 2.52 days, the relative error becomes positive (a pattern of overshooting in the testing period), and the magnitude of the error increases when the latency period increases. Hence, we expect that when the latency period is between 2 and 2.52 days, the relative error will change its sign with a further reduced magnitude, and there is possibly a critical value for the latency period that minimizes the error.

To verify this, we have chosen a number of additional values between 2 and 2.52 days for the latency period, and repeatedly run the fitting and testing steps for each case. Figure 9 shows the relative errors in the testing period for a few typical scenarios, with latency periods of 2.30, 2.35, 2.40 and 2.45 days. As expected, the error in each of these scenarios has a very small magnitude and crosses the horizontal axis. To quantify the difference, we have also computed the L_1 norm (i.e., the absolute sum) of the error over the 30-day testing period for each case, and found that the L_1 norm of the error is minimized when the latency period is 2.40 days (see Figure 9).

Furthermore, as a comparison, we add the parameter v into the set of parameters to be fitted by data, and conduct the fitting and testing procedure again for the SEAIR model. Now we need to estimate four

parameters: β_A, β_I, w, and v, in the fitting period, and the results are provided in Table 6. In this case, we see that the latency period directly estimated from data is $v^{-1} \approx 5$ days. The comparison between the simulation results and the actual data and the calculation of the relative error in the testing period are presented in Figure 10. We clearly observe that the accuracy of the prediction in Figure 10 is lower than that in Figure 9. The implication is that this approach of directly fitting the latency period from data, though efficient, may not be as accurate in the predictions as the previous approach of indirectly (and repeatedly) calibrating the latency period.

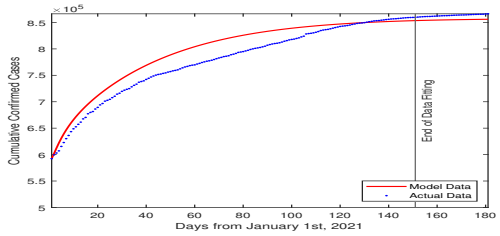

(A) Latency period = 1 day

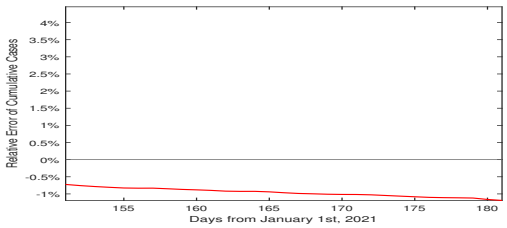

(B) Latency period = 1 day

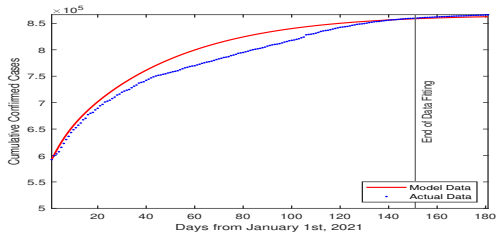

(C) Latency period = 2 days

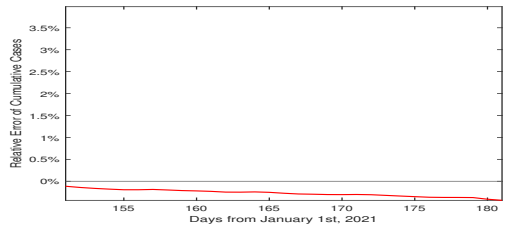

(D) Latency period = 2 days

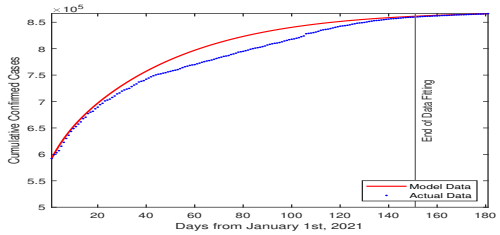

(E) Latency period = 2.52 days

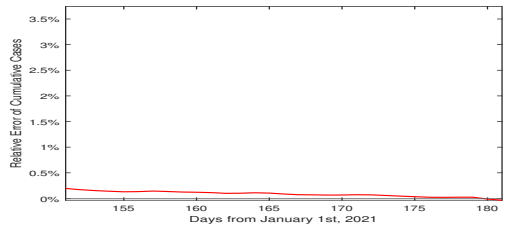

(F) Latency period = 2.52 days

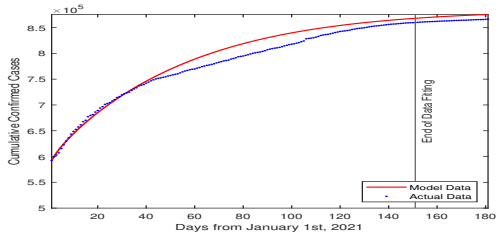

(G) Latency period = 4 days

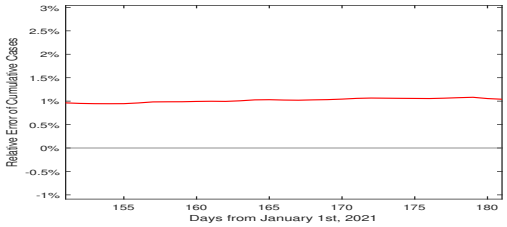

(H) Latency period = 4 days

FIGURE 8. Actual data and simulation results for the cumulative cases using latency periods of 1, 2, 2.52 and 4 days. The left panel shows the comparisons in both the fitting and testing periods, and the right panel shows the relative errors in the testing period.

TABLE 6. Parameter estimates involving latency

Parameter	Resultant Value	95% Confidence Interval
β_A	2.96×10^{-8}/person/day	$(2.42 \times 10^{-8}, 3.08 \times 10^{-8})$
β_I	4.72×10^{-9}/person/day	$(4.55 \times 10^{-9}, 4.90 \times 10^{-9})$
w	0.012/day	(0.004, 0.020)
v	0.201/day	(0.148, 0.255)

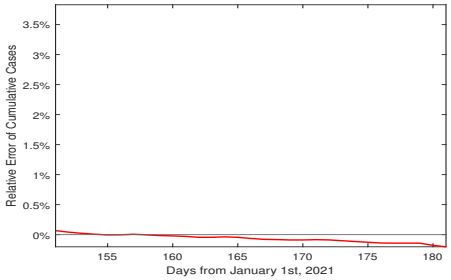

(A) Latency period = 2.30 days

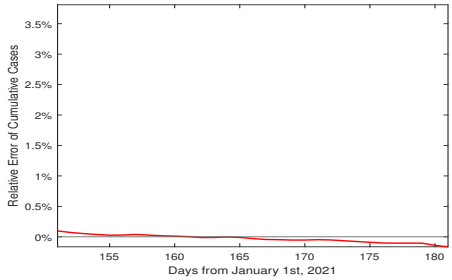

(B) Latency period = 2.35 days

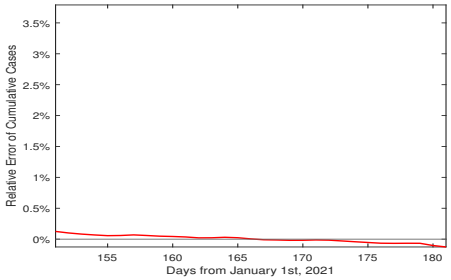

(C) Latency period = 2.40 days

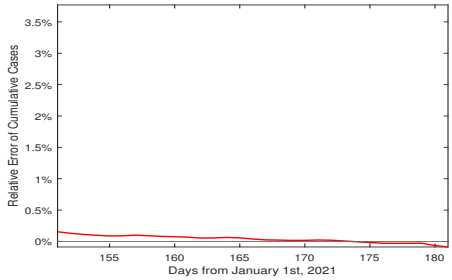

(D) Latency period = 2.45 days

FIGURE 9. Relative errors between actual data and simulation results in the testing period for the cumulative cases: (A) Latency period = 2.30 days, L_1 norm of error = 0.02252; (B) Latency period = 2.35 days, L_1 norm of error = 0.01725; (C) Latency period = 2.40 days, L_1 norm of error = 0.01555; (D) Latency period = 2.45 days, L_1 norm of error = 0.01780.

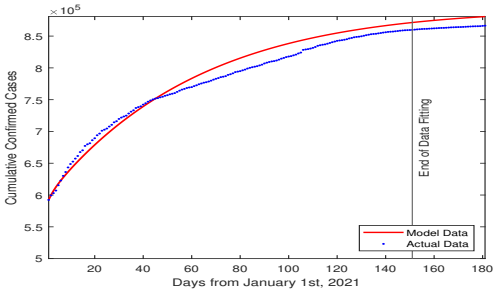

(A) Latency period = 1/0.201 days

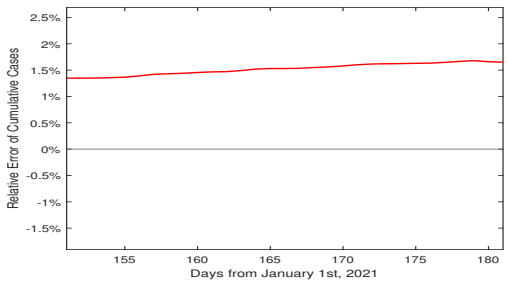

(B) Latency period = 1/0.201 days

FIGURE 10. Actual data and simulation results for the cumulative cases with the latency period directly fitted from data: (a) comparisons in both the fitting and testing periods; and (b) relative error in the testing period.

Additionally, we list in Table 7 the values of the basic reproduction number ($\mathcal{R}_0^{\text{SEAIR}}$) and its two components ($\mathcal{R}_1^{\text{SEAIR}}$ and $\mathcal{R}_2^{\text{SEAIR}}$) for each different choice of the latency period discussed in this section. Note that each latency period here corresponds to a different set of fitted parameters β_A, β_I, and w (see Table 5). Hence, we see a larger variation of the basic reproduction numbers than that presented in Table 4.

TABLE 7. Basic reproduction numbers for different fitting scenarios

Latency Period	$\mathcal{R}_1^{\text{SEAIR}}$	$\mathcal{R}_2^{\text{SEAIR}}$	$\mathcal{R}_0^{\text{SEAIR}}$
0.1 days	0.549	0.321	0.870
1 day	0.555	0.322	0.877
2 days	0.564	0.321	0.885
2.30 days	0.566	0.322	0.888
2.35 days	0.566	0.322	0.888
2.40 days	0.566	0.322	0.888
2.45 days	0.566	0.323	0.889
2.52 days	0.566	0.323	0.889
3 days	0.566	0.326	0.892
4 days	0.569	0.330	0.899

5. DISCUSSION

We have performed a modeling study for the impact of the latency period on the transmission dynamics of COVID-19, by considering an SAIR model and an SEAIR model and comparing their dynamical behaviors. Each model incorporates the dual (asymptomatic and symptomatic) transmission routes of COVID-19, but the second model (SEAIR) additionally includes a latent compartment that is absent from the first one (SAIR). For model comparison, we have combined equilibrium analysis, asymptotic study, and numerical simulation.

Using the COVID-19 data in the state of Tennessee, we have examined various scenarios associated with different latency periods in this work. In particular, our findings show that within the biologically meaningful regime, the dynamics of the SEAIR model approach those of the SAIR model when the length of the latency period tends to 0. Meanwhile, we have numerically tested several values of the latency period and found that when the latency period equals 2.40 days, the predictions generated by the SEAIR model achieve the best performance in the sense that the relative error is minimized over the testing period. This numerically found 'optimal' value is close to the mean latency period of 2.52 days estimated in the meta-analysis of COVID-19 data from seven countries [22].

Among our numerical findings, we highlight the following: (1) The value of the latency period has a substantial impact on the state variables, particularly the numbers of the asymptomatic and symptomatic infectious cases generated by the models. (2) The latency period has a less significant impact on the basic reproduction number. In this regard, using the SAIR model or the SEAIR model with different latency periods to evaluate the basic reproduction number would lead to similar results. (3) The accuracy of the predictions from the SEAIR model strongly depends on the latency period, and a carefully calibrated value of the latency period could minimize the error of the prediction. These results could provide useful guidelines in the selection of mathematical models and calibration of parameters to study the transmission and spread of COVID-19.

Although some of the findings in this work are specific to the COVID-19 data in Tennessee, the methodology can be generalized toward broader applications. As is common in data fitting studies,

potential inaccuracy of the data could impact the quantitative outcome of our models, though we expect that our qualitative predictions would still hold. By presenting two very basic and simple models, we have adopted the point of view that "useful models are simple and extendable" [11]. The two models (SAIR and SEAIR) are analytically tractable and their dynamics can be compared through both asymptotic and numerical studies, which serve our main purpose of investigating the interplay between the asymptomatic and symptomatic transmission routes and the latency period in COVID-19 transmission dynamics. On the other hand, we have only discussed the local asymptotic stability of the equilibrium solutions (Appendices B and C) and have not studied the global stability properties, since the stability of the dynamical systems is not our focus in this work. Nevertheless, standard techniques, such as the geometric approach [18] and Lyapunov functions, can be employed to conduct the global stability analysis when needed. Moreover, our modeling framework can be extended in a number of ways by incorporating factors such as disease prevention and intervention measures, SARS-CoV-2 variants, and hospitalization. We expect, however, that the qualitative relationship between a model incorporating the latency period and one without considering latency would remain the same. An additional remark is that we have not explicitly considered vaccination in our current models. Instead, the impact of vaccination is implicitly incorporated into the models through the diseases transmission rates whose values fitted from real data could (at least) partially reflect the reduced infection risk due to vaccine deployment.

Appendix A: Basic reproduction numbers

We first consider the SAIR model (2.1). It is straightforward to determine that the disease-free equilibrium (DFE) of the system is $x_0 = (\Lambda/\mu, 0, 0, 0)$. To find the basic reproduction number of the system, $\mathcal{R}_0^{\text{SAIR}}$, we use the next-generation matrix method described by Driessche and Watmough [31]. To do this, we define two vectors, $\mathscr{F}$ and $\mathscr{V}$, where $\mathscr{F}$ represents the rate at which new infection is introduced in the asymptomatic and symptomatic compartments and $\mathscr{V}$ represents the rate of transfer into and out of these compartments. Thus we obtain

$$\begin{bmatrix} \frac{dA}{dt} \\ \frac{dI}{dt} \end{bmatrix} = \mathscr{F} - \mathscr{V} = \begin{bmatrix} \beta_A SA + \beta_I SI \\ 0 \end{bmatrix} - \begin{bmatrix} (\alpha+\gamma_1+\mu)A \\ (w+\gamma_2+\mu)I - \alpha A \end{bmatrix}.$$

Now we find the Jacobians of $\mathscr{F}$ and $\mathscr{V}$ at the DFE,

$$F = \left[\tfrac{\partial \mathscr{F}}{\partial x}(x_0)\right] = \begin{bmatrix} \beta_A\Lambda/\mu & \beta_I\Lambda/\mu \\ 0 & 0 \end{bmatrix},$$

$$V = \left[\tfrac{\partial \mathscr{V}}{\partial x}(x_0)\right] = \begin{bmatrix} \alpha+\gamma_1+\mu & 0 \\ -\alpha & w+\gamma_2+\mu \end{bmatrix}.$$

This gives us the next-generation matrix

$$FV^{-1} = \begin{bmatrix} \frac{\beta_A\Lambda}{\mu(\alpha+\gamma_1+\mu)} + \frac{\alpha\beta_I\Lambda}{\mu(\alpha+\gamma_1+\mu)(w+\gamma_2+\mu)} & \frac{\beta_I\Lambda}{\mu(w+\gamma_2+\mu)} \\ 0 & 0 \end{bmatrix}.$$

The basic reproduction number is then defined as the spectral radius of the next-generation matrix FV^{-1}. So

$$\mathcal{R}_0^{\text{SAIR}} = \frac{\beta_A\Lambda}{\mu(\alpha+\gamma_1+\mu)} + \frac{\alpha\beta_I\Lambda}{\mu(\alpha+\gamma_1+\mu)(w+\gamma_2+\mu)}. \tag{A.1}$$

Next, we consider the SEAIR model (2.3). The DFE of the system is given by $x_0 = (\Lambda/\mu, 0, 0, 0, 0)$. To find the basic reproduction number, $\mathcal{R}_0^{\text{SEAIR}}$, we similarly separates the system into two parts:

$$\begin{bmatrix} \frac{dE}{dt} \\ \frac{dA}{dt} \\ \frac{dI}{dt} \end{bmatrix} = \mathscr{F} - \mathscr{V} = \begin{bmatrix} \beta_A SA + \beta_I SI \\ 0 \\ 0 \end{bmatrix} - \begin{bmatrix} (v+\mu)E \\ (\alpha+\gamma_1+\mu)A - vE \\ (w+\gamma_2+\mu)I - \alpha A \end{bmatrix}.$$

The Jacobians of $\mathscr{F}$ and $\mathscr{V}$ evaluated at the DFE are

$$F = \left[\frac{\partial \mathscr{F}}{\partial x}(x_0)\right] = \begin{bmatrix} 0 & \beta_A\Lambda/\mu & \beta_I\Lambda/\mu \\ 0 & 0 & 0 \\ 0 & 0 & 0 \end{bmatrix},$$

$$V = \left[\frac{\partial \mathscr{V}}{\partial x}(x_0)\right] = \begin{bmatrix} v+\mu & 0 & 0 \\ -v & (\alpha+\gamma_1+\mu) & 0 \\ 0 & -\alpha & (w+\gamma_2+\mu) \end{bmatrix}.$$

Thus the next-generation matrix is

$$FV^{-1} = \begin{bmatrix} \frac{v\beta_A\Lambda}{\mu(v+\mu)(\alpha+\gamma_1+\mu)} + \frac{v\alpha\beta_I\Lambda}{\mu(v+\mu)(\alpha+\gamma_1+\mu)(w+\gamma_2+\mu)} & \frac{\beta_A\Lambda}{\mu(\alpha+\gamma_1+\mu)} + \frac{\alpha\beta_I\Lambda}{\mu(\alpha+\gamma_1+\mu)(w+\gamma_2+\mu)} & \frac{\beta_I\Lambda}{\mu(w+\gamma_2+\mu)} \\ 0 & 0 & 0 \\ 0 & 0 & 0 \end{bmatrix}.$$

Consequently, the spectral radius of the matrix FV^{-1} yields

$$\mathcal{R}_0^{\text{SEAIR}} = \frac{v\beta_A\Lambda}{\mu(v+\mu)(\alpha+\gamma_1+\mu)} + \frac{v\alpha\beta_I\Lambda}{\mu(v+\mu)(\alpha+\gamma_1+\mu)(w+\gamma_2+\mu)}. \tag{A.2}$$

Appendix B: Equilibrium analysis for the SAIR model

An equilibrium point of the SAIR system (2.1) implies that $\frac{dS}{dt} = \frac{dA}{dt} = \frac{dI}{dt} = \frac{dR}{dt} = 0$ and so should satisfy the following equations

$$\Lambda = \beta_A SA + \beta_I SI + \mu S, \tag{B.1}$$

$$(\alpha+\gamma_1+\mu)A = \beta_A SA + \beta ISI, \tag{B.2}$$

$$0 = \alpha A - (w+\gamma_2+\mu)I, \tag{B.3}$$

$$0 = \gamma_1 A + \gamma_2 I - \mu R. \tag{B.4}$$

We show that when $\mathcal{R}_0^{\text{SAIR}} < 1$ the only equilibrium point is the DFE, and when $\mathcal{R}_0^{\text{SAIR}} > 1$ there exists a positive endemic equilibrium. Firstly, we rewrite equation (B.3) so that A is expressed as a function of I:

$$A(I) = \frac{(w+\gamma_2+\mu)I}{\alpha} \tag{B.5}$$

which is increasing for all $I > 0$. Next, we substitute the right-hand side of equation (B.2) into equation (B.1) to get

$$\Lambda = (\alpha+\gamma_1+\mu)A(I) + \mu S$$

and from this we derive

$$S(I) = \frac{\Lambda - (\alpha+\gamma_1+\mu)A(I)}{\mu}, \tag{B.6}$$

which is decreasing since $A(I)$ is increasing.

By substituting equation (B.5) into equation (B.2), we obtain

$$\frac{(\alpha+\gamma_1+\mu)(w+\gamma_2+\mu)I}{\alpha} = \frac{\beta_A S(I)(w+\gamma_2+\mu)I}{\alpha} + \beta_I S(I)I.$$

When $I \neq 0$, this simplifies into

$$1 = S(I)\left(\tfrac{\beta_A}{\alpha+\gamma_1+\mu} + \tfrac{\beta_I\alpha}{(\alpha+\gamma_1+\mu)(w+\gamma_2+\mu)}\right). \tag{B.7}$$

We denote the right-hand side of equation (B.7) by $f(I)$, which is decreasing since $S(I)$ is decreasing. Clearly, $f(I) < 1$ for sufficiently large I. Therefore, to guarantee that a unique endemic equilibrium exists, $f(0) > 1$ must be true, where

$$f(0) = S(0)\left(\tfrac{\beta_A}{\alpha+\gamma_1+\mu} + \tfrac{\beta_I\alpha}{(\alpha+\gamma_1+\mu)(w+\gamma_2+\mu)}\right) = \frac{\Lambda}{\mu}\left(\tfrac{\beta_A}{\alpha+\gamma_1+\mu} + \tfrac{\beta_I\alpha}{(\alpha+\gamma_1+\mu)(w+\gamma_2+\mu)}\right). \tag{B.8}$$

By equation (A.1), we have $f(0) = \mathcal{R}_0^{\mathrm{SAIR}}$. This implies that when $\mathcal{R}_0^{\mathrm{SAIR}} > 1$, there is a unique endemic equilibrium, and when $\mathcal{R}_0^{\mathrm{SAIR}} < 1$, the only possible equilibrium is the DFE.

Based on the standard result in [31], the unique DFE is locally asymptotically stable when $\mathcal{R}_0^{\mathrm{SAIR}} < 1$ and unstable when $\mathcal{R}_0^{\mathrm{SAIR}} > 1$. Next, we use the Routh-Hurwitz criteria to show that the unique endemic equilibrium is locally asymptotically stable when $\mathcal{R}_0^{\mathrm{SAIR}} > 1$.

Firstly, we let $\widehat{X} = (\widehat{S}, \widehat{A}, \widehat{I}, \widehat{R})$ be the unique endemic equilibrium, and construct the Jacobian of the system at the endemic equilibrium:

$$J = \begin{bmatrix} -\beta_A\widehat{A} - \beta_I\widehat{I} - \mu & -\beta_A\widehat{S} & -\beta_I\widehat{S} & 0 \\ \beta_A\widehat{A} + \beta_I\widehat{I} & \beta_A\widehat{S} - \alpha - \gamma_1 - \mu & \beta_I\widehat{S} & 0 \\ 0 & \alpha & -(w+\gamma_2+\mu) & 0 \\ 0 & 0 & \gamma_1+\gamma_2 & -\mu \end{bmatrix}.$$

Next we find the eigenvalues using the characteristic polynomial defined by $\det(\lambda I - J) =$

$$(\lambda+\mu)\begin{vmatrix} \lambda + (\beta_A\widehat{A} + \beta_I\widehat{I} + \mu) & \beta_A\widehat{S} & \beta_I\widehat{S} \\ -\beta_A\widehat{A} - \beta_I\widehat{I} & \lambda - (\beta_A\widehat{S} - \alpha - \gamma_1 - \mu) & -\beta_I\widehat{S} \\ 0 & -\alpha & \lambda + (w+\gamma_2+\mu) \end{vmatrix}$$

which, for simplicity, we denote as

$$(\lambda+\mu)\begin{vmatrix} \lambda + a_{11} & a_{12} & a_{13} \\ a_{21} & \lambda + a_{22} & a_{23} \\ 0 & -\alpha & \lambda + a_{33} \end{vmatrix}.$$

This gives us the characteristic equation

$$(\lambda+\mu)(\lambda^3 + x\lambda^2 + y\lambda + z) \tag{B.9}$$

where

$$x = a_{11} + a_{22} + a_{33}, \tag{B.10}$$

$$y = a_{23}\alpha + a_{11}(a_{22} + a_{33}) + a_{22}a_{33} - a_{21}a_{12}, \tag{B.11}$$

$$z = a_{11}a_{22}a_{33} - a_{21}a_{12}a_{33} + \alpha(a_{11}a_{23} - a_{21}a_{13}). \tag{B.12}$$

To satisfy the Routh-Hurwitz criteria and prove local asymptotic stability, we need to show that $x > 0$, $y > 0$, $z > 0$, and $xy > z$. We start off by showing that $x > 0$. It is simple to confirm that each component of x is positive:

$$a_{11} = \beta_A\widehat{A} + \beta_I\widehat{I} + \mu, \tag{B.13}$$

which is clearly positive, and

$$a_{33} = w + \gamma_2 + \mu, \tag{B.14}$$

which is also positive. Using equation (B.2), $(\beta_A\widehat{S}-\alpha-\mu)$ can be rewritten as $\frac{-\beta_I\widehat{S}\widehat{I}}{\widehat{A}}$, therefore

$$a_{22}=\frac{\beta_I\widehat{S}\widehat{I}}{\widehat{A}}, \tag{B.15}$$

so a_{22} is positive as well. Since each component of x is positive, we conclude that $x>0$.

Next we show that $y>0$. It is clear that since a_{11}, a_{22} and a_{33} are all positive, $a_{11}(a_{22}+a_{33})$ is positive as well. Now, $-a_{21}a_{12}>0$ since

$$-a_{21}a_{12}=-(-\beta_A\widehat{A}-\beta_I\widehat{I})(\beta_A\widehat{S})=(\beta_A\widehat{A}+\beta_I\widehat{I})(\beta_A\widehat{S}).$$

Finally, we look at $a_{23}\alpha+a_{22}a_{33}$. Using equation (B.3), a_{33} can be rewritten as

$$a_{33}=(w+\gamma_2+\mu)=\frac{\alpha\widehat{A}}{\widehat{I}}. \tag{B.16}$$

Therefore, using the value of a_{22} given by equation (B.15),

$$a_{23}\alpha+a_{22}a_{33}=-\beta_I\widehat{S}\alpha+\frac{\beta_I\widehat{S}\widehat{I}}{\widehat{A}}(\frac{\alpha\widehat{A}}{\widehat{I}})=0,$$

giving us a new equation for y,

$$y=a_{11}(a_{22}a_{33})-a_{21}a_{12}, \tag{B.17}$$

which allows us to conclude $y>0$.

Now we show that $z>0$. To begin, we look at $\alpha(a_{11}a_{23}-a_{21}a_{13})$:

$$\begin{aligned}\alpha(a_{11}a_{23}-a_{21}a_{13})&=\alpha((\beta_A\widehat{A}+\beta_I\widehat{I}+\mu)(-\beta_I\widehat{S})-(-\beta_A\widehat{A}-\beta_I\widehat{I})(\beta_I\widehat{S}))\\&=\alpha(-(\beta_A\widehat{A}+\beta_I\widehat{I})(\beta_I\widehat{S})+(\beta_A\widehat{A}+\beta_I\widehat{I})(\beta_I\widehat{S})-\mu\beta_I\widehat{S})\\&=-\mu\beta_I\widehat{S}\alpha\,.\end{aligned} \tag{B.18}$$

Using this result and the product of $a_{11}a_{22}a_{33}$, and using the values of a_{22} and a_{33} from equations (B.15) and (B.16), respectively, we can see that

$$a_{11}a_{22}a_{33}+\alpha(a_{11}a_{23}-a_{21}a_{13})=(\beta_A\widehat{A}+\beta_I\widehat{I})(\beta_I\widehat{S}\alpha),$$

which is clearly positive. Now,

$$\begin{aligned}-a_{21}a_{12}a_{33}&=-(-\beta_A\widehat{A}-\beta_I\widehat{I})(\beta_A\widehat{S})(\frac{\alpha\widehat{A}}{\widehat{I}})\\&=(\beta_A\widehat{A}+\beta_I\widehat{I})(\beta_A\widehat{S})(\frac{\alpha\widehat{A}}{\widehat{I}})\end{aligned},$$

which is also positive. Therefore, since each component of z is positive, we can conclude that $z>0$.

Finally, we need to verify that $xy>z$. To do this, we need to look at $a_{33}y$:

$$\begin{aligned}a_{33}y&=(\frac{\alpha\widehat{A}}{\widehat{I}})((\beta_A\widehat{A}+\beta_I\widehat{I}+\mu)(\frac{\beta_I\widehat{S}\widehat{I}}{\widehat{A}}+\frac{\alpha\widehat{A}}{\widehat{I}})+(\beta_A\widehat{A}+\beta_I\widehat{I})(\beta_A\widehat{S}))\\&=(\beta_A\widehat{A}+\beta_I\widehat{I})(\beta_I\widehat{S}\alpha)+(\beta_A\widehat{A}+\beta_I\widehat{I})(\beta_A\widehat{S})(\frac{\alpha\widehat{A}}{\widehat{I}})+(\beta_A\widehat{A}+\beta_I\widehat{I})(\frac{\alpha\widehat{A}}{\widehat{I}})^2+\mu(\beta_I\widehat{S}\alpha+(\frac{\alpha\widehat{A}}{\widehat{I}})^2).\end{aligned}$$

This is greater than z because $z=(\beta_A\widehat{A}+\beta_I\widehat{I})(\beta_I\widehat{S}\alpha)+(\beta_A\widehat{A}+\beta_I\widehat{I})(\beta_A\widehat{S})(\frac{\alpha\widehat{A}}{\widehat{I}})$, and since $x>a_{33}$, we conclude that $xy>z$.

Thus, all of the Routh-Hurwitz criteria are satisfied, and we conclude that the unique endemic equilibrium is locally asymptotically stable when it exists; i.e., when $\mathcal{R}_0^{\text{SAIR}}>1$.

Appendix C: Equilibrium analysis for the SEAIR model

An equilibrium of the SEAIR system (2.3) should satisfy

$$\Lambda = \beta_A SA + \beta_I SI + \mu S, \tag{C.1}$$

$$(v+\mu)E = \beta_A SA + \beta_I SI, \tag{C.2}$$

$$0 = vE - (\alpha + \gamma_1 + \mu)A, \tag{C.3}$$

$$0 = \alpha A - (w + \gamma_2 + \mu)I, \tag{C.4}$$

$$0 = \gamma_1 A + \gamma_2 I - \mu R. \tag{C.5}$$

Using equation (C.4) we get

$$A(I) = \frac{(w+\gamma_2+\mu)I}{\alpha}, \tag{C.6}$$

and by equation (C.3) we get

$$E(I) = \frac{(\alpha+\gamma_1+\mu)(w+\gamma_2+\mu)I}{v\alpha}, \tag{C.7}$$

both of which are increasing for all $I > 0$.

Substituting equation (C.6) into equation (C.1), we have

$$S(I) = \frac{\Lambda}{\frac{\beta_A(w+\gamma_2+\mu)I}{\alpha} + \beta_I I + \mu}, \tag{C.8}$$

which is decreasing for all $I > 0$. Next, we substitute equations (C.6) and (C.7) into equation (C.2) to obtain

$$1 = S(I)\left(\frac{\beta_A v}{(v+\mu)(\alpha+\gamma_1+\mu)} + \frac{\beta_I v\alpha}{(v+\mu)(\alpha+\gamma_1+\mu)(w+\gamma_2+\mu)}\right),$$

the right-hand side of which is denoted by $f(I)$. Now, $f(I)$ is decreasing since $S(I)$ is decreasing for all $I > 0$ and $f(I) < 1$ for sufficiently large I. Thus, to guarantee a unique endemic equilibrium, $f(0) > 1$ must be true, where

$$f(0) = \frac{\Lambda}{\mu}\left(\frac{\beta_A v}{(v+\mu)(\alpha+\gamma_1+\mu)} + \frac{\beta_I v\alpha}{(v+\mu)(\alpha+\gamma_1+\mu)(w+\gamma_2+\mu)}\right), \tag{C.9}$$

which is identical to $\mathcal{R}_0^{\text{SEAIR}}$. Thus, we conclude that when $\mathcal{R}_0^{\text{SEAIR}} < 1$ the only equilibrium point is the DFE, and when $\mathcal{R}_0^{\text{SEAIR}} > 1$, there exists a unique positive endemic equilibrium.

Next, as in the SAIR model, we use the Routh-Hurwitz criteria to show that the endemic equilibrium of the SEAIR model is locally asymptotically stable when $\mathcal{R}_0^{\text{SEAIR}} > 1$. Let $\widehat{X} = (\widehat{S}, \widehat{E}, \widehat{A}, \widehat{I}, \widehat{R})$ be the unique endemic equilibrium for the system. We construct the Jacobian, J, of the system at the endemic equilibrium:

$$J = \begin{bmatrix} -\beta_A\widehat{A} - \beta_I\widehat{I} - \mu & 0 & -\beta_A\widehat{S} & -\beta_I\widehat{S} & 0 \\ \beta_A\widehat{A} + \beta_I\widehat{I} & -(v+\mu) & \beta_A\widehat{S} & \beta_I\widehat{S} & 0 \\ 0 & v & -(\alpha+\gamma_1+\mu) & 0 & 0 \\ 0 & 0 & \alpha & -(w+\gamma_2+\mu) & 0 \\ 0 & 0 & \gamma_1 & \gamma_2 & -\mu \end{bmatrix}.$$

To determine the characteristic polynomial, we compute

$$\det(I\lambda - J) = (\lambda+\mu)\begin{vmatrix} \lambda + \beta_A\widehat{A} + \beta_I\widehat{I} + \mu & 0 & \beta_A\widehat{S} & \beta_I\widehat{S} \\ -\beta_A\widehat{A} - \beta_I\widehat{I} & \lambda + (v+\mu) & -\beta_A\widehat{S} & -\beta_I\widehat{S} \\ 0 & -v & \lambda + (\alpha+\gamma_1+\mu) & 0 \\ 0 & 0 & -\alpha & \lambda + (w+\gamma_2+\mu) \end{vmatrix},$$

which for simplicity we denote as

$$(\lambda+\mu)\begin{vmatrix} \lambda+a_{11} & 0 & a_{13} & a_{14} \\ a_{21} & \lambda+a_{22} & a_{23} & a_{24} \\ 0 & -v & \lambda+a_{33} & 0 \\ 0 & 0 & -\alpha & \lambda+a_{44} \end{vmatrix}.$$

This gives us the characteristic polynomial

$$(\lambda+\mu)(\lambda^4+x\lambda^3+y\lambda^2+z\lambda+c), \tag{C.10}$$

where

$$x = a_{11}+a_{22}+a_{33}+a_{44}, \tag{C.11}$$

$$y = va_{23}+a_{11}a_{22}+a_{11}a_{33}+a_{11}a_{44}+a_{22}a_{33}+a_{22}a_{44}+a_{33}a_{44}, \tag{C.12}$$

$$z = v\alpha a_{24}+va_{23}a_{44}+va_{11}a_{23}-a_{21}a_{13}+a_{11}a_{22}a_{33}+a_{22}a_{33}a_{44} + a_{11}a_{33}a_{44}+a_{11}a_{22}a_{44}, \tag{C.13}$$

$$c = a_{11}(va_{44}a_{23}+v\alpha a_{24})-v\alpha a_{21}a_{14}-va_{44}a_{21}a_{13}+a_{11}a_{22}a_{33}a_{44}. \tag{C.14}$$

To verify the Routh-Hurwitz criteria for stability, we need to show $x>0$, $y>0$, $z>0$, $c>0$, and $xyz>z^2+cx^2$.

To begin, we already know $x=a_{11}+a_{22}+a_{33}+a_{44}$ is positive since each of our parameters is assumed to be positive. Now, to show that y is positive we need to look at va_{23}:

$$va_{23} = -v\beta_A\widehat{S}.$$

Substituting equations (C.6) and (C.7) into equation (C.2), we can get

$$-v\beta_A\widehat{S} = \frac{v\alpha\beta_I\widehat{S}}{(w+\gamma_2+\mu)}-(v+\mu)(\alpha+\gamma_1+\mu). \tag{C.15}$$

The latter term of this, $-(v+\mu)(\alpha+\gamma_1+\mu)$, is equal to $-a_{22}a_{33}$ so the terms will cancel out. We are left with

$$y = \frac{v\alpha\beta_I\widehat{S}}{(w+\gamma_2+\mu)}+a_{11}a_{22}+a_{11}a_{33}+a_{11}a_{44}+a_{22}a_{44}+a_{33}a_{44}, \tag{C.16}$$

which is clearly positive.

To show that $z>0$, we first need to look at the terms $v\alpha a_{24}+va_{23}a_{44}$:

$$v\alpha a_{24}+va_{23}a_{44} = -v\alpha\beta_I\widehat{S}-v\beta_A\widehat{S}(w+\gamma_2+\mu)$$

Substituting equations (C.6) and (C.7) into equation (C.2) yields

$$-v\alpha\beta_I\widehat{S} = v\beta_A\widehat{S}(w+\gamma_2+\mu)-(v+\mu)(\alpha+\gamma_1+\mu)(w+\gamma_2+\mu). \tag{C.17}$$

Therefore,

$$v\alpha a_{24}+va_{23}a_{44} = -(v+\mu)(\alpha+\gamma_1+\mu)(w+\gamma_2+\mu),$$

which will cancel with the term $a_{22}a_{33}a_{44}$. Next, we have

$$va_{11}a_{23} = -v\beta_A\widehat{S}(\beta_A\widehat{A}+\beta_I\widehat{I}+\mu),$$

which can be rewritten using equation (C.15) to be

$$va_{11}a_{23} = \frac{v\alpha\beta_I\widehat{S}}{(w+\gamma_2+\mu)}(\beta_A\widehat{A}+\beta_I\widehat{I}+\mu)-(v+\mu)(\alpha+\gamma_1+\mu)(\beta_A\widehat{A}+\beta_I\widehat{I}+\mu)$$

which cancels out the term $a_{11}a_{22}a_{33}$, and we are left with $\frac{v\alpha\beta_I\widehat{S}}{(w+\gamma_2+\mu)}(\beta_A\widehat{A}+\beta_I\widehat{I}+\mu)$, which is clearly positive. Finally, the last term in question is

$$-a_{21}a_{13} = (\beta_A\widehat{A}+\beta_I\widehat{I})(\beta_A\widehat{S}),$$

which is also clearly positive. After all the canceling terms we are left with

$$z = \frac{v\alpha\beta_I\widehat{S}}{(w+\gamma_2+\mu)}a_{11} - a_{21}a_{13} + a_{11}a_{33}a_{44} + a_{11}a_{22}a_{44}, \tag{C.18}$$

every term of which is positive, and so we conclude that $z > 0$.

Next, we need to show that $c > 0$. Firstly, we know the terms $-v\alpha a_{21}a_{14} - va_{44}a_{21}a_{14}$ are positive since

$$-v\alpha a_{21}a_{14} - va_{44}a_{21}a_{14} = v\alpha(\beta_A\widehat{A}+\beta_I\widehat{I})(\beta_I\widehat{S}) + v(\beta_A\widehat{A}+\beta_I\widehat{I})(\beta_A\widehat{S})(w+\gamma_2+\mu).$$

Secondly, we have $a_{11}(v\alpha a_{24} + va_{23}a_{44})$, which, using equation (C.17), can be written as

$$a_{11}(v\alpha a_{24} + va_{23}a_{44}) = -(\beta_A\widehat{A}+\beta_I\widehat{I}+\mu)(v+\mu)(\alpha+\gamma_1+\mu)(w+\gamma_2+\mu),$$

which will cancel out with $a_{11}a_{22}a_{33}a_{44}$. Thus, we are left with

$$c = -v\alpha a_{21}a_{14} - va_{44}a_{21}a_{13}, \tag{C.19}$$

and we conclude that $c > 0$.

Finally, we may conduct similar calculations to show $xyz > z^2 + cx^2$, though the algebraic manipulations become very tedious and the details are not provided here. Verification of all these Routh-Hurwitz criteria will lead to our conclusion that the endemic equilibrium of the SEAIR model is locally asymptotically stable when it exists; i.e., when $\mathcal{R}_0^{\text{SEAIR}} > 1$.

Appendix D: Sensitivity of the basic reproduction number

To quantify the influence of model parameters in shaping the disease risk, we conduct a sensitivity analysis for the basic reproduction numbers of the SAIR and SEAIR models. This is usually achieved by evaluating the relative sensitivity. To compute the relative sensitivity of the basic reproduction number, $\mathcal{R}_0$, in terms of a parameter, h, we take the partial derivative of $\mathcal{R}_0$ with respect to h, and then normalize the result by dividing it with the quotient $\mathcal{R}_0/h$. That is,

$$\frac{\partial\mathcal{R}_0}{\partial h}\cdot\frac{h}{\mathcal{R}_0},$$

and we substitute the parameter values from data fitting (Section 4) to complete the evaluation of the relative sensitivity. This procedure is applied to each parameter that the basic reproduction number depends on.

Figures 11 and 12 show the sensitivity analysis results for the SAIR mode and the SEAIR model, respectively.

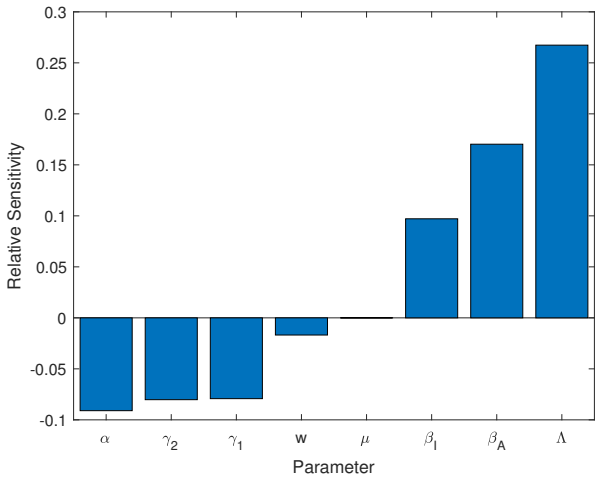

FIGURE 11. Sensitivity analysis results for the basic reproduction number of the SAIR model.

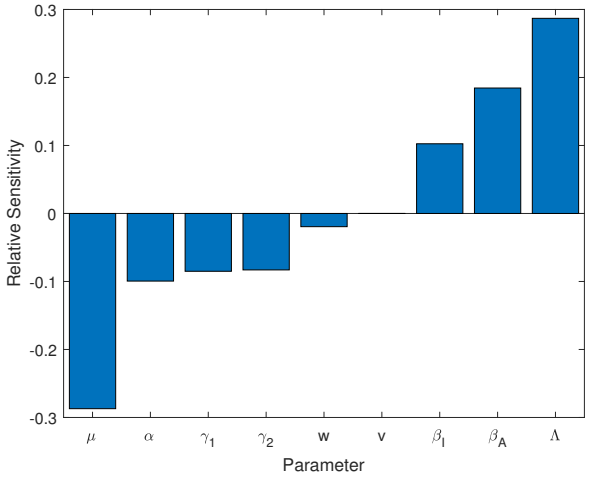

FIGURE 12. Sensitivity analysis results for the basic reproduction number of the SEAIR model.

REFERENCES

[1] E. Arias, B. Bastian, J. Xu, and B. Tejada-Vera, *U.S. State Life Tables, 2018*, National Vital Statistics Reports, **70**(2021).

[2] G.K. Batchelor, *An Introduction to Fluid Dynamics*, Cambridge University Press, 1967.

[3] C.M. Bender and S.A. Orszag, *Advanced Mathematical Methods for Scientists and Engineers*, Springer, 1999.

[4] F. Brauer, *Mathematical epidemiology: Past, present, and future*, Infectious Disease Modelling, **2**(2017), 113-127.

[5] F. Brauer, *A singular perturbation approach to epidemics of vector-transmitted diseases*, Infectious Disease Modelling, **4**(2019), 115-123.

[6] F. Brauer and C. Castillo-Chavez, *Mathematical Models in Population Biology and Epidemiology*, Springer, 2001.

[7] M. Brown, M. Jiang, C. Yang, and J. Wang, *Modeling cholera transmission under disease control measures*, Journal of Biological Systems, **29**(2021), 219-244.

[8] A.W. Byrne, D. McEvoy, A.B. Collins, et al., *Inferred duration of infectious period of SARS-CoV-2: rapid scoping review and analysis of available evidence for asymptomatic and symptomatic COVID-19 cases*, BMJ Open, **10**(2021), e039856.

[9] C. Cheng, D. Zhang, D. Dang, et al., *The incubation period of COVID-19: a global meta-analysis of 53 studies and a Chinese observation study of 11,545 patients*, Infectious Diseases of Poverty, **10**(2021), 119.
[10] Z.J. Cheng and J. Shan, *2019 Novel Coronavirus: where we are and what we know*, Infection, **48**(2020), 155-163.
[11] K.Z. Coyte, H. Tabuteau, E.A. Gaffney, K.R. Foster, and W.M. Durham, *Reply to Baveye and Darnault: Useful models are simple and extendable*, Proceedings of the National Academy of Sciences, **114**(2017), E2804-E2805.
[12] G. He, W. Sun, P. Fang, J. Huang, M. Gamber, J. Cai, and J. Wu, *The clinical feature of silent infections of novel coronavirus infection (COVID-19) in Wenzhou*, Journal of Medical Virology, **92**(2020), 1761-1763.
[13] H.W. Hethcote, *The mathematics of infectious diseases*, SIAM Review, **42**(2000), 599-653.
[14] E.J. Hinch, *Perturbation Methods*, Cambridge University Press, 1991.
[15] M.H. Holmes, *Introduction to Perturbation Methods*, Springer, 1995.
[16] N. Imai, A. Cori, I. Dorigatti, M. Baguelin, C.A. Donnelly, S. Riley, and N.M. Ferguson, *Report 3: Transmissibility of 2019-nCoV*, published online January 25, 2020. Available at https://www.imperial.ac.uk/mrc-global-infectious-disease-analysis/news--wuhan-coronavirus/
[17] K. Leung, J.T. Wu, D. Liu, and G.M. Leung, *First-wave COVID-19 transmissibility and severity in China outside Hubei after control measures, and second-wave scenario planning: a modelling impact assessment*, Lancet, **395**(2020), 1382-1393.
[18] M.Y. Li and J.S. Muldowney, *A geometric approach to global-stability problems*, SIAM Journal on Mathematical Analysis, **27**(1996), 1070-1083.
[19] R. Li, S. Pei, B. Chen, Y. Song, T. Zhang, W. Yang, and J. Shaman, *Substantial undocumented infection facilitates the rapid dissemination of novel coronavirus (SARS-CoV2)*, Science, **368**(2020), 489-493.
[20] Z. Liu, P. Magal, O. Seydi, and G. Webb, *A COVID-19 epidemic model with latency period*, Infectious Disease Modelling, **5**(2020), 323-337.
[21] Q.B. Lu, Y. Zhang, M.J. Liu, et al., *Epidemiological parameters of COVID-19 and its implication for infectivity among patients in China, 1 January to 11 February 2020*, Euro surveillance, **25**(2020), 2000250.
[22] S. Ma, J. Zhang, M. Zeng, Q. Yun, W. Guo, et al., *Epidemiological parameters of coronavirus disease 2019: a pooled analysis of publicly reported individual data of 1155 cases from seven countries*, medRxiv, 2020. DOI: https://doi.org/10.1101/2020.03.21.20040329
[23] J.D. Murray, *Mathematical Biology*, Springer, 2002.
[24] M. Pollán, B. Pérez-Gómez, R. Pastor-Barriuso, J. Oteo, M.A. Hernán, M. Pérez-Olmeda, et al., *Prevalence of SARS-CoV-2 in Spain (ENE-COVID): a nationwide, population-based seroepidemiological study*, Lancet, **396**(2020), 535-544.
[25] B. Rai, A. Shukla, and L.K. Dwivedi, *Incubation period for COVID-19: a systematic review and meta-analysis*, Journal of Public Health: From Theory to Practice, 2021.
[26] C. Rothe, M. Schunk, P. Sothmann, G. Bretzel, G. Froeschl, et al., *Transmission of 2019-nCoV infection from an asymptomatic contact in Germany*, New England Journal of Medicine, **382**(2020), 970-971.
[27] L. Sadun, *Effects of latency on estimates of the COVID-19 replication number*, Bulletin of Mathematical Biology, **82**(2020), 114.
[28] A. Sahin, A. Erdogan, P. Mutlu Agaoglu, Y. Dineri, A. Cakirci, M. Senel, R. Okyay, and A. Tasdogan, *2019 Novel Coronavirus (COVID-19) outbreak: a review of the current literature*, Eurasian Journal of Medicine and Oncology, **4**(2020), 1-7.
[29] B. Tang, X. Wang, Q. Li, N.L. Bragazzi, S. Tang, Y. Xiao, and J. Wu, *Estimation of the transmission risk of 2019-nCoV and its implication for public health interventions*, Journal of Clinical Medicine, **9**(2020), 462.
[30] H.R. Thieme, *Mathematics in Population Biology*, Princeton University Press, 2003.
[31] P. van den Driessche and J. Watmough, *Reproduction numbers and sub-threshold endemic equilibria for compartmental models of disease transmission*, Mathematical Biosciences, **180**(2001), 29-48.
[32] F. Verhulst, *Methods and Applications of Singular Perturbations: Boundary Layers and Multiple Timescale Dynamics*, Springer, 2005.
[33] J. Wang, *Mathematical models for COVID-19: applications, limitations, and potentials*, Journal of Public Health and Emergency, **4**(2020), 9.
[34] J.T. Wu, K. Leung, and G.M. Leung, *Nowcasting and forecasting the potential domestic and international spread of the 2019-nCoV outbreak originating in Wuhan, China: a modelling study*, Lancet, **395**(2020), 689-697.
[35] H. Xin, Y. Li, P. Wu, et al., *Estimating the latent period of coronavirus disease 2019 (COVID-19)*, Clinical Infectious Diseases, ciab746, 2021.
[36] C. Yang and J. Wang, *A mathematical model for the novel coronavirus epidemic in Wuhan, China*, Mathematical Biosciences and Engineering, **17**(2020), 2708-2724.

[37] C. Yang and J. Wang, *Modeling the transmission of COVID-19 in the US – A case study*, Infectious Disease Modelling, **6**(2021), 195-211.
[38] Centers for Disease Control and Prevention: Coronavirus Disease 2019 (COVID-19). Available at https://www.cdc.gov/coronavirus/2019-ncov
[39] Centers for Disease Control and Prevention: COVID-19 Pandemic Planning Scenarios. Available at https://www.cdc.gov/coronavirus/2019-ncov/hcp/planning-scenarios.html
[40] Datasets from Tennessee Department of Health. Available at https://www.tn.gov/health/cedep/ncov/data/downloadable-datasets.html
[41] Tennessee Department of Health. Available at https://www.tn.gov/health.html
[42] U.S. Census Bureau Quick Facts: Tennessee. Available at https://www.census.gov/quickfacts/fact/table/TN
[43] WHO Coronavirus Disease (COVID-19) Weekly Epidemiological Update and Weekly Operational Update. Available at https://www.who.int/emergencies/diseases/novel-coronavirus-2019/situation-reports

Department of Mathematics, University of Tennessee at Chattanooga, Chattanooga, TN 37403, USA
Email address: gvj998@mocs.utc.edu

Corresponding author, Department of Mathematics, University of Tennessee at Chattanooga, Chattanooga, TN 37403, USA
Email address: Jin-Wang02@utc.edu